SPE 131772

New Pore-scale Considerations for Shale Gas in Place Calculations

Ray J. Ambrose, Devon Energy and The University of Oklahoma, Robert C. Hartman, Weatherford Labs,
Mery Diaz-Campos, I. Yucel Akkutlu, and Carl H. Sondergeld, The University of Oklahoma

This paper was prepared for presentation at the SPE Unconventional Gas Conference held in Pittsburgh, Pennsylvania, USA, 23–25 February 2010.

Abstract

Using FIB/SEM imaging technology, a series of 2-D and 3-D submicro-scale investigations are performed on the types of porous constituents inherent to gas shale. A finely-dispersed porous organic (kerogen) material is observed imbedded within an inorganic matrix. The latter may contain larger-size pores of varying geometries although it is the organic material that makes up the majority of gas pore volume, with pores and capillaries having characteristic lengths typically less than 100 nanometers. A significant portion of total gas in-place appears to be associated with inter-connected large nano-pores within the organic material.

This observation has several implications on reservoir engineering of gas shales. Primarily, thermodynamics (phase behavior) of fluids in these pores are known to be quite different. Most importantly, gas residing in a small pore or capillary is rarefied under the influence of organic pore walls and shows a density profile across the pore with damped-oscillations. This raises the following serious questions related to gas-in-place calculations: under reservoir conditions, what fraction of the pore volume of the organic material can be considered available for the free gas phase and what fraction is taken up by the adsorbed phase? If a significant fraction of the organic pore volume is taken up by the adsorbed phase, how accurately is the shale gas storage capacity estimated using the conventional volumetric methods? And, finally, do average densities exist for the free and the adsorbed phases and how large would a typical density contrast be in an organic pore for an accurate gas reserve calculation?

In order to answer these questions we combine the Langmuir equilibrium adsorption isotherm with the volumetrics for free gas and formulate a new gas-in-place equation accounting for the organic pore space taken up by the sorbed phase. The method yields a total gas-in-place prediction based on a corrected free gas pore volume that is obtained using an average adsorbed gas density. Next, we address the fundamental-level questions related to phase transition in organic matter using equilibrium molecular dynamics simulations involving methane in small carbon slit-pores of varying size and temperature. We predict methane density profiles across the pores and show that (i) an average total thickness for an adsorbed methane layer is typically 0.7 nm, which is roughly equivalent to 4% of a 100 nm diameter pore volume, and (ii) the adsorbed phase density is 1.8-2.0 times larger than that of the bulk methane, i.e., in the absence of pore wall effects. These findings suggest that a significant level of adjustment is necessary in volume calculations, especially for gas shales high in total organic content. Finally, using typical values for the parameters, we perform a series of calculations using the new volumetric method and show a 10-25% decrease in total gas storage capacity compared to that using the conventional approach. This additionally could have a larger impact in shales where the sorbed gas phase is a more significant portion of the total gas-in-place. The new methodology is recommended for estimating shale gas-in-place and the approach could be extended to other unconventional gas-in-place calculations where both sorbed and free gas phases are present.

1. Introduction

When conducting a reservoir study on a natural gas field, one of the primary concerns is the estimation of initial gas in-place. The estimate is the basis for disclosure of gas reserves and it is important for reservoir engineering analysis such as gas production forecasts. Tank-type and multi-dimensional (simulation-based) material balance calculations are common industry approaches in predicting the gas in-place when sufficient field performance data is available. To gain confidence in the estimate, or when sufficient data is not available to initiate the material balance calculations, the volumetric methods are applied. Using key reservoir parameters (i.e., porosity, water saturation and formation volume factor) associated with well-logs, core data, fluid samples and well tests, a volumetric method allows us to predict the gas-in-place in terms of a total gas

pore volume of the reservoir.

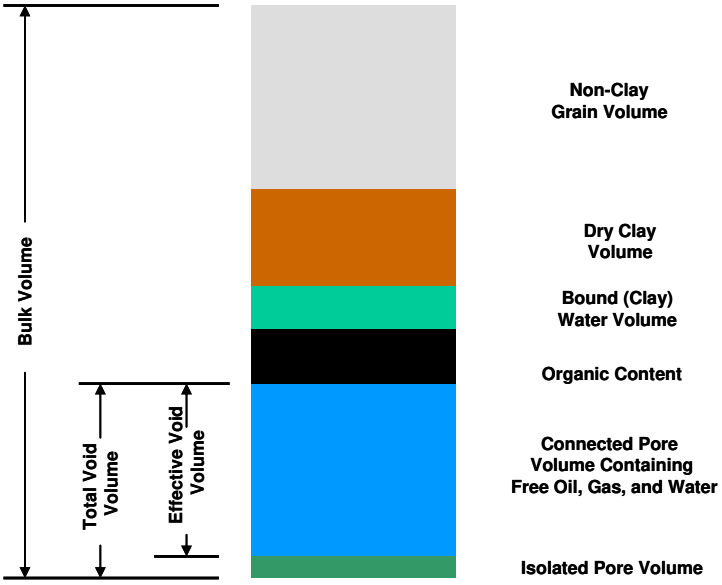

Fig. 1. Petrophysical model conceptually showing the volumetric constituents of a shale matrix.

For disclosure purposes, a deterministic volumetric method, in which a single average value is selected for each parameter in the reserves calculations, is most commonly used in North America. Probabilistic methods, on the other hand, are increasingly used worldwide and give the ability to describe the full range of values for each parameter in order to somewhat reflect spatial variability in the parameters and structural intricacies in reservoir architecture. In this paper it is shown that any volumetric approach for shale gas reserves estimation has added complexity because in shale the natural gas (mostly methane) exists in different thermodynamic states, namely adsorbed, absorbed (or dissolved) and free gas, and that an accurate estimation of the gas pore volume in shale reservoirs should not be considered independent of these thermodynamic states of the gas.

A simple model of a typical shale physical matrix is illustrated in **Fig. 1**. The model needs to be quantified for gas-in-place analysis and it is typically done by methods developed specifically for tight rocks and other low-permeability formations (Luffel et. al 1992, Luffel at. al. 1993, GRI 1997). However, the effective pore volume is not directly determined in these studies; rather a total porosity, total water volume, and total oil volume (by weight difference and an assumed oil density of 0.8g/cc) are determined. Nonetheless, as shown here in equations (1) and (2), the total and effective gas porosity values are equivalent:

$$\phi S_g = (V_v/V_b)(V_g/V_v) = V_g/V_b \quad (1)$$

$$\phi S_{ge} = (V_{ve}/V_b)(V_g/V_{ve}) = V_g/V_b \quad (2)$$

Bulk volume V_b in equations (1) and (2) is determined by mercury displacement of competent core. Grain volume, on the other hand, is determined on crushed core via helium porosimetry. The difference between these two volumes yields the total void volume V_v (associated with total porosity ϕ) available for all in-situ fluids, i.e. mobile hydrocarbons, free and bound water, adsorbed gas, solution gas, and free gas.

For total gas storage, the shale gas-in-place volumes are generally considered in terms of the following:

- A volumetric component, G_f, involving hydrocarbons stored in the pore space as free gas. The free gas volume is quantified by modifications of standard reservoir evaluation methods.
- A surface component, G_a, with the gas physically adsorbed on large surface area of the micropores. Adsorbed gas amount has generally been quantified from the sorption isotherm measurements by establishing an equilibrium adsorption isotherm.

- A volumetric component, G_{so}, involving gas dissolved into the liquid hydrocarbon. This volume is usually combined with adsorbed gas capacity in reservoirs that contain a large fraction of liquid hydrocarbon in the pore space.
- A volumetric component, G_{sw}, involving gas dissolved into the formation water. The amount of dissolved gas is estimated from the bulk solubility calculations. Although it has traditionally not been considered important, a recent study is available discussing significant enhancement in gas solubility in formation liquids when confined to small pores (Diaz-Campos et al. 2009).

Hence, we have G_{st} as the total gas in-place:

$$G_{st} = G_f + G_a + G_{so} + G_{sw} \tag{3}$$

where:

$$G_f = 32.0368 \frac{\phi(1 - S_w - S_o)}{\rho_b B_g} \tag{4}$$

$$G_a = G_{sL} \frac{p}{p + p_L} \tag{5}$$

$$G_{so} = \frac{32.0368}{5.6146} \frac{\phi S_o R_{so}}{\rho B_o} \tag{6}$$

$$G_{sw} = \frac{32.0368}{5.6146} \frac{\phi S_w R_s}{\rho B_w} \tag{7}$$

In the current industry standard calculations, equations (6) and (7) are not applied. The solution gas in mobile hydrocarbons and water, and the adsorbed gas within organic matter are combined in the adsorption isotherm analysis; therefore equation (3) reduces to:

$$G_{st} = G_f + G_a \tag{8}$$

Note that G_f is equivalent to equations (1) or (2) although, to be consistent with the total gas sorption data G_a, it is now defined in equation (4) in terms of standard cubic feet per ton (GRI, 1997).

The current volumetric approaches for shale gas are built on the premise that the two volumes on the right hand side of equation (8), being associated with the inorganic pores and organic solid, respectively, can be estimated independently of one-another. Accordingly, the sorbed gas is associated with the organics, the pore volume of which is considered to be negligible and, therefore, the volume does not need to be accounted for during the calculations of free gas; whereas, all of the free gas is associated with the inorganic macropores, fissures, fractures etc. In this paper, based on new pore-scale observations, we argue that the total gas storage capacities and the resulting gas in-place values are being inadvertently inflated and overestimated by this point of view. The source of the error involves the proper accounting of the volume occupied by the sorbed gas phase. Cui et. al. (2009) addresses sorbed phase porosity and its effects on transport processes; this work is an extension.

2. Sorbed Phase Correction for the Void Volume

The amount of sorbed gas that is estimated to be in shale is determined through an equilibrium adsorption isotherm experiment. In this experiment, a void volume is first measured, typically using helium. Void volume determination is experimentally identical to the helium porosimetry techniques used to determine grain density. [Some authors have raised the issue of molecular size (Bustin et. al. 2008) as a source of error; this error will not be discussed here.] After the void volume has been measured, the sorption data are collected. The mass of gas sorbed into the sample is measured by material balance and a given thermodynamic equation-of-state. During construction of the isotherm, at each pressure step, the volume of the gas that is adsorbed reduces the void volume. As a result, the initially determined void volume must be corrected at the beginning and end of the pressure step as described in equations (9) and (10) (Menon, 1968).

$$V_{v1} = V_{v0} - \frac{n_1 \hat{M}}{\rho_s} \tag{9}$$

$$V_{v2} = V_{v0} - \frac{n_2 \hat{M}}{\rho_s} \tag{10}$$

Accordingly, over the course of the isotherm analysis, the void volume is further reduced for each subsequent pressure step. In practice, it is often more convenient to determine a so-called Gibbs isotherm in terms of number of moles of adsorbed gas, equation (11).

$$n'_2 = n'_1 + V_r \left(\frac{p_{r1}}{z_{r1} R T_{r1}} - \frac{p_{r2}}{z_{r2} R T_{r2}} \right) + V_{v0} \left(\frac{p_{s1}}{z_{s1} R T_{s1}} - \frac{p_{s2}}{z_{s2} R T_{s2}} \right) \tag{11}$$

The Gibbs isotherm can then be converted to volumes using an equation-of-state and can be adjusted for the void volume using the Gibbs correction factor ρ_f/ρ_s:

$$G_a = \frac{G'_a}{1 - \frac{\rho_f}{\rho_s}} \tag{12}$$

If the changes in void volume are not taken into account, the isotherm will be in error and not usable in engineering calculations. An example of isotherm data with and without void volume corrections is shown in **Fig. 2**. The aforementioned void volume considerations that are necessary to accurately determine adsorbed gas volumes have significant implications on the "live," in-situ shale pore volume available for free gas storage. Simply put, the effective porosity gas saturation product (ϕS_{ge}) is derived from a total pore volume that is determined under static lab conditions and does not reflect live reservoir conditions. The reservoir portion of the total pore volume is not only consumed by water and oil but also by the adsorbed gas. It is for this reason we propose that the calculated free gas pore volume requires a correction for the adsorbed gas fraction present under reservoir temperature and pressure conditions.

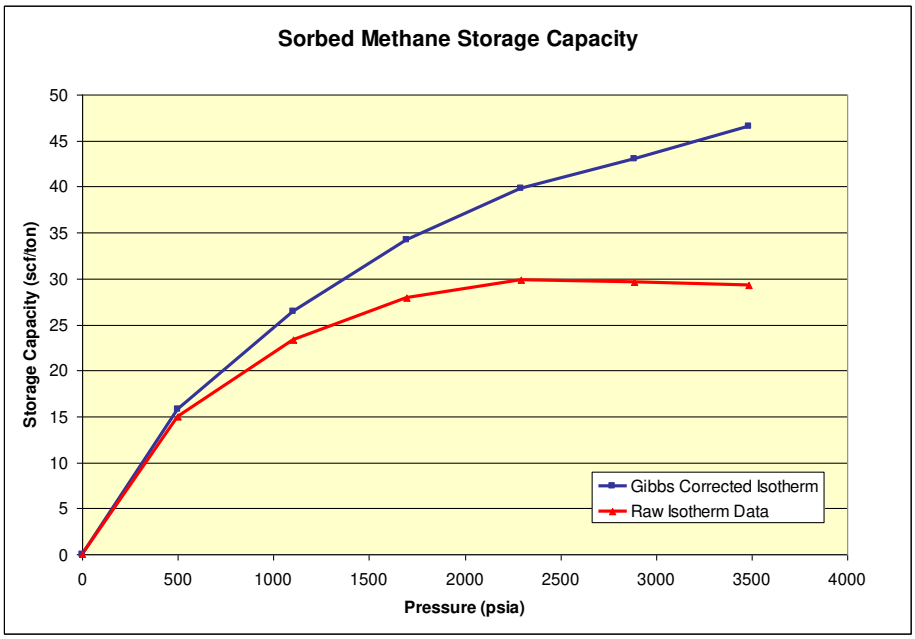

Fig. 2. Methane isotherms with and without Gibbs correction.

Additional evidence to support the need for the correction lies in visual investigation of the complex rock fabric typical of fine-grained, organic-rich shales. It has recently been reported that much of the gas storage capacity within shale is thought to be predominately associated with the organic fraction of the rock matrix (Loucks et al. 2009; Wang and Reed 2009; Sondergeld et al. 2010). Therefore, the free gas volumes measured by pycnometry using a non-adsorbent gas such as helium must be corrected for the presence of adsorbed gas within the organics. **Fig. 3** shows a 2D focused ion beam SEM gas shale image supporting the previous observations. In the image, the matrix is represented by the gray color, dark- and light-gray regions being the organic (kerogen) and the inorganic constituents (clay, silica, feldspar, etc.), respectively; whereas, the pores are shown in black. Clearly, most of the pores are significantly small, typically less than 100 nm, and are almost exclusively found within the kerogen.

Using advanced imaging technologies; we have created 3-D shale segmentations showing kerogen- and pore-networks that contain up to 600 such FIB/SEM images. A typical kerogen network of our study is shown in **Fig. 4**. The network consists of large inter-connected pockets of kerogen, which makes up an estimated 7.7% (vol.) of the segment. **Fig. 5** shows the superimposed kerogen- (bounded with yellow) and pore- (on red) networks of the same shale segment. As can be seen again from these images, nearly all of the porosity within the system is associated with the kerogen network. The image-computed porosity for this segmented volume is 2.5%. A 3-D network overlay showing the comparison of the kerogen/pore networks and the gray-scale image is shown in **Fig. 6** (orange denotes kerogen, dark orange denotes pore).

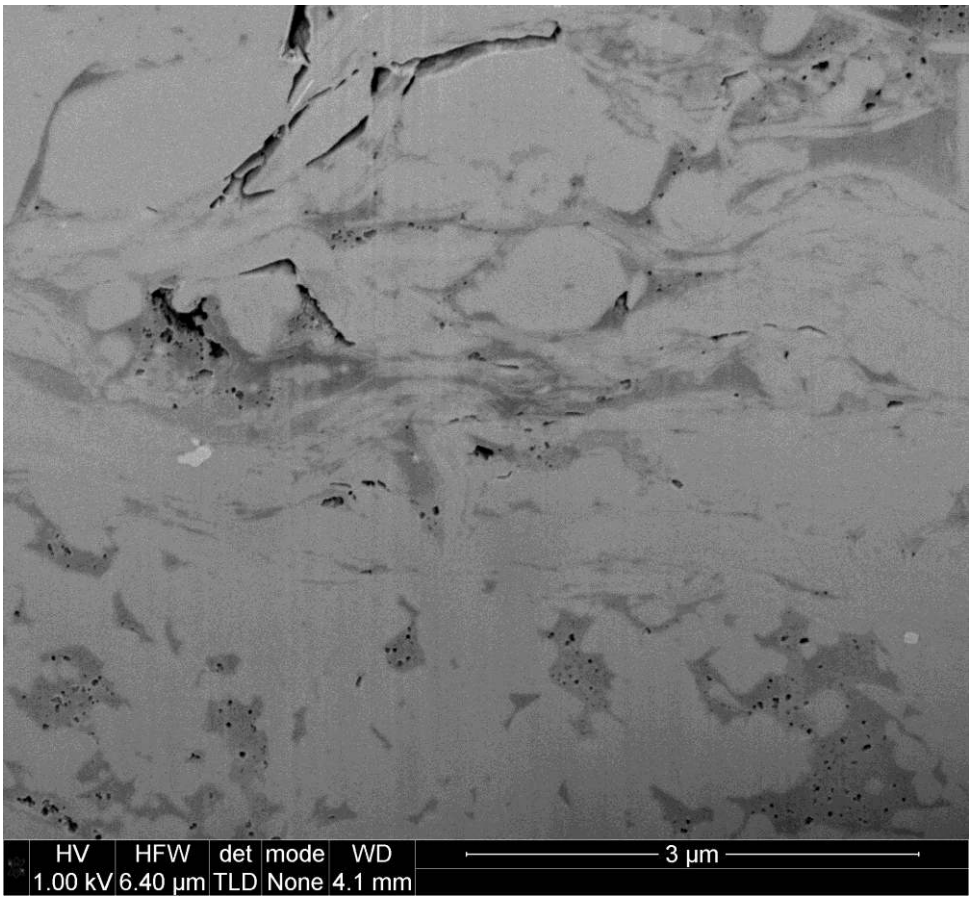

Fig. 3. 2-D FIB/SEM image showing porosity and kerogen within shale. Black depicts pore, dark gray is kerogen, light gray is matrix (clay and silica).

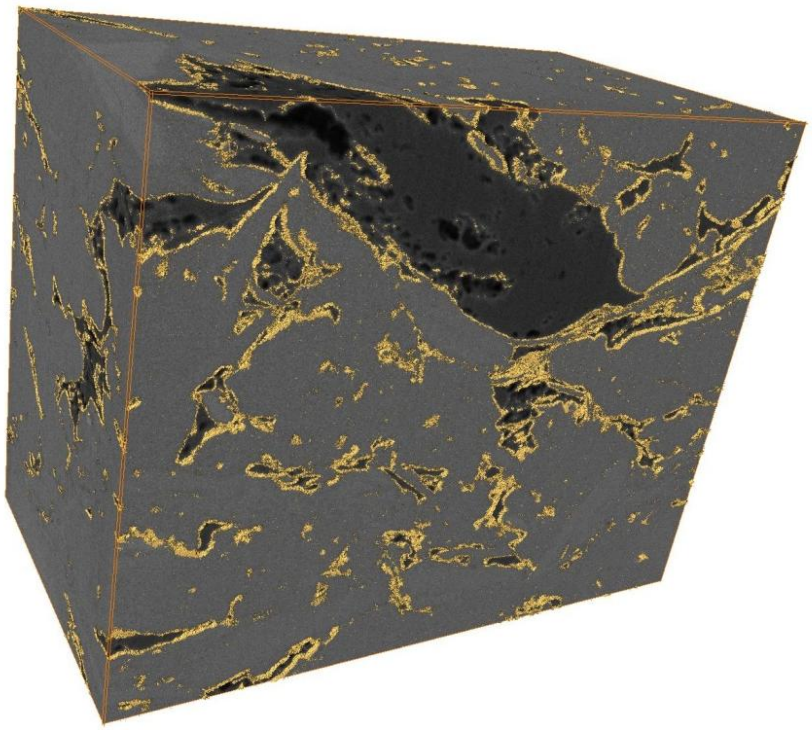

Fig. 4. 3-D FIB/SEM segmentation showing kerogen network, yellow outlines the 3-D kerogen network. Sample size is 4 μm high, 5 μm wide and 2.5 μm deep.

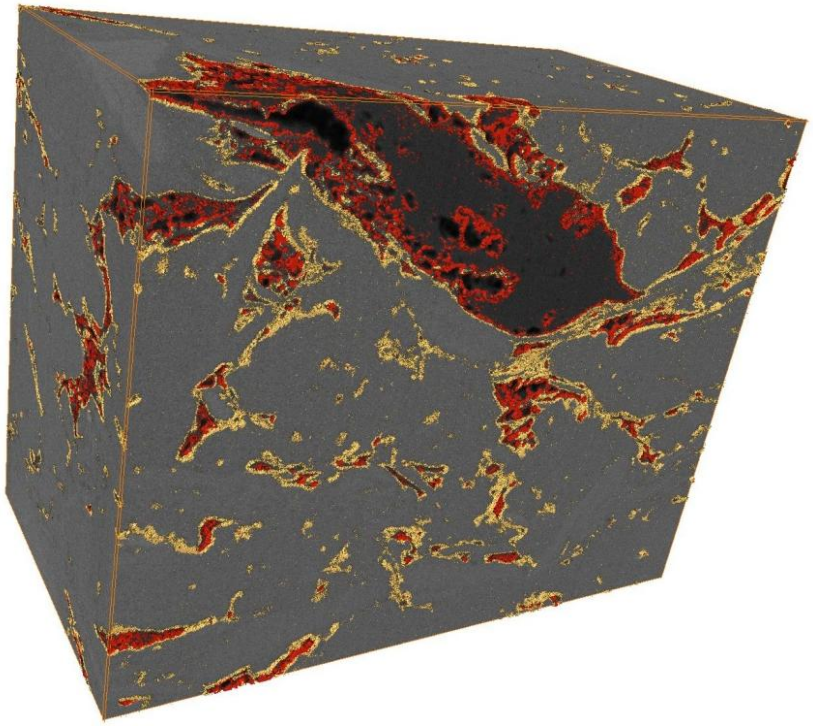

Fig. 5. 3-D FIB/SEM segmentation showing porosity and kerogen network, yellow outlines 3-D kerogen network, red outlines porosity (in this sample all porosity is found within the kerogen).

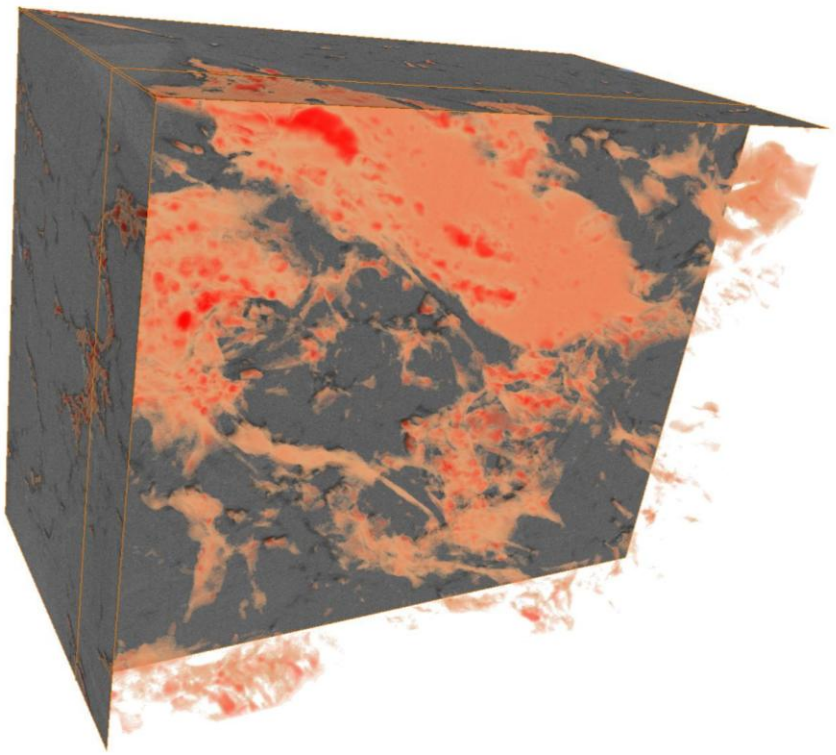

Fig. 6. Overlay of porosity and kerogen 3-D network on 2-D image; orange is kerogen network, dark orange depicts porosity within kerogen. Notice difference in left portion of sample compared to Fig. 5. The large orange mass (kerogen and pore) is further in depth than what can bee seen on the surface in Fig. 5.

3. Method for Shale Gas in-place Calculations

In this paper, a new petrophysical model is proposed that alters the previous concept of effective porosity earlier shown in Fig. 1. The new model shown in **Fig. 7** emphasizes two distinct conceptual changes with respect to the previous model. First, there exists a dependency of the connected pore space on the organics (Wang 2009; Loucks et.al. 2009; Sondergeld et. al. 2010). Second, there is a dependency on the free pore space by the inclusion of a sorbed phase. **Fig. 8** shows a simple diagram of the current methodology used to determine gas in-place vs. the proposed methodology. (For simplicity, the water and oil volumes are not considered in the diagram.) The simple illustration taken in context with the new information from the FIB/SEM images and segmentations visually shows the errors by assuming that the sorbed gas takes up no volume.

In order to properly account for the total and free gas-in-place, the volume consumed by the adsorbed gas must be determined and subtracted from the free gas calculation. We therefore propose the standard calculations utilized to calculate free gas storage capacity (equation 4) should be modified as:

$$G_f = \frac{32.0368}{B_g}\left[\frac{\phi(1-S_w)}{\rho_b} - \frac{1.318\times10^{-6}\hat{M}}{\rho_s}\left(G_{sL}\frac{p}{p+p_L}\right)\right] \tag{13}$$

The volume occupied by the sorbed gas must be accounted for after the correction for water saturation. This is due to the porosity basis of the water saturation measurement. See **Appendix A** for the derivation of equation (13).

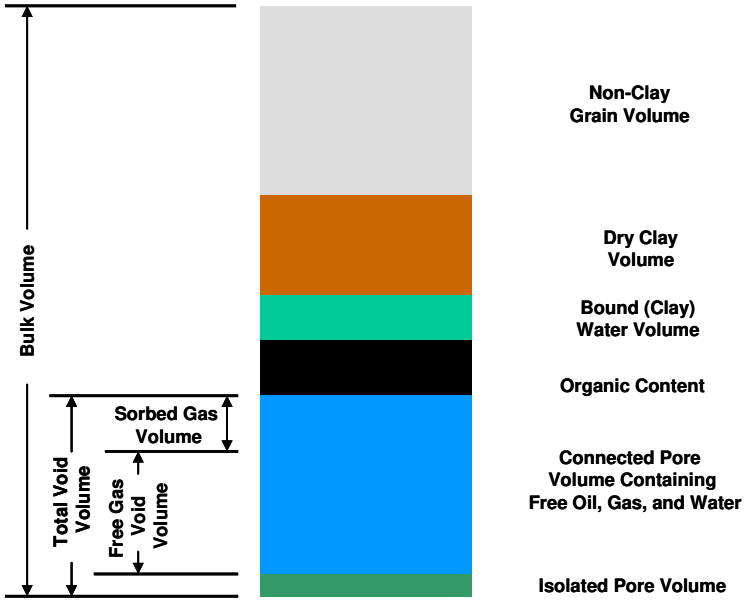

Fig. 7. New petrophysical model showing volumetric constituents of gas-shale matrix. The hashed region describes the interplay between the sorbed phase and total porosity (void volume).

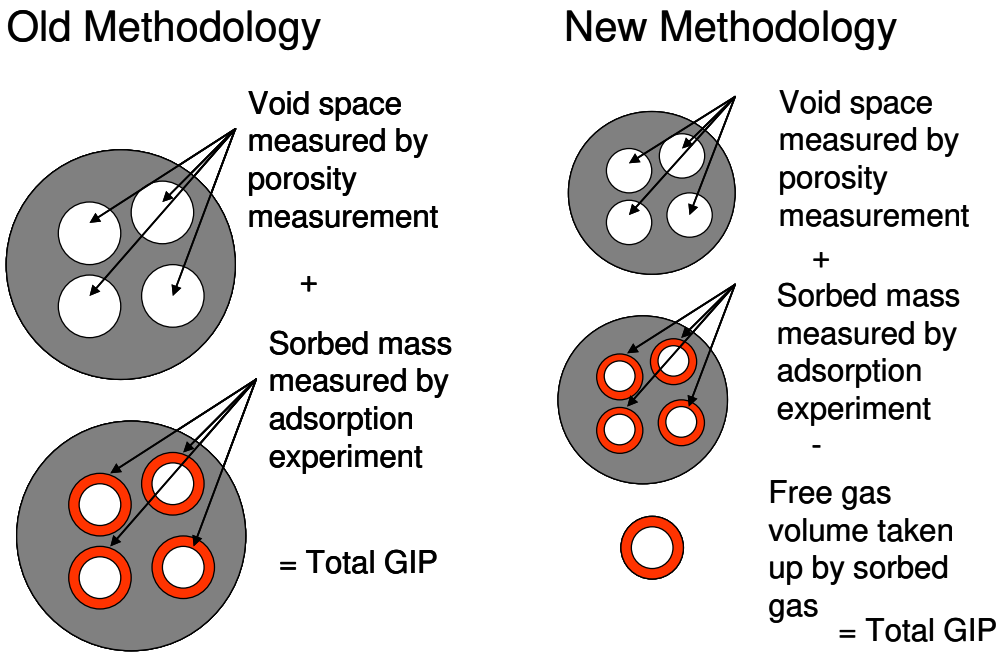

Fig. 8. Comparison of the old and new methodologies in predicting shale gas in-place.

3.1. Sorbed Phase Density

In order to calculate the volume occupied by the sorbed phase, the density of adsorbed gas in the organic pores must be known. Measurement of the sorbed phase density is not a trivial matter, however, the local density for methane is expected to vary across the pore and to be different from its average bulk density due to the added interactions between methane and the organic walls. Further, in gas shales where the reservoir temperature is significantly greater than the supercritical temperature of the natural gas, it is difficult to study phase transitions and determine if the adsorbate is in the form of a liquid or vapor. There have been several suggestions in the chemistry literature to determine the density of the adsorbed phase on solid surfaces.

Dubinin, (1960) suggested that the adsorbate density is related to the van der Waals co-volume constant, *b*. Independently,

Haydel and Kobayashi, (1967) used an experimental method and found the density values for methane and propane to be nearly equal to the van der Waals co-volume constant. Later, it was argued that the sorbed gas density is equivalent to the liquid density, (Menon, 1968), and to the critical density, (Tsai et al. 1985), of the sorbed gas. Ozawa (1976) considered the adsorbed phase as a superheated liquid with a density dependant upon the thermal expansion of the liquid. Recently Ming et al. (2002) compared all of the previously stated methods to a Langmuir-Freundlich adsorption model and found that there exists a temperature-dependence to the sorbed phase density, but the value approaches those proposed by Dubinin (1960). These studies, although fundamentally important to our understanding of gas adsorption in shale, do not show a clear and accurate path to estimate the adsorbed phase density of shale gas, hence, gas-in-place.

In this study, we used a numerical molecular modeling approach to determine the adsorbed phase density from the first principles of Newtonian mechanics. Molecular simulations have made enormous strides in recent years and are gradually becoming a commonly used tool in science and engineering (de Pablo and Escobedo, 2002). Today, molecular simulations are being widely used to construct virtual experiments in cases where controlled laboratory measurements are difficult, if not impossible, to perform. There exists an exhaustive literature studying the equilibrium thermodynamics of fluids using molecular simulation involving phase change of bulk fluids (Harris, 1995), characterization of porous materials using gas adsorption (Aukett, 1992; Sweatman and Quirke, 2001), and multi-component gas separation (Hamon et al., 2009; Ghoufi, 2009). In our case, two sets of molecular dynamics (MD) simulations are used to estimate and analyze the adsorbed phase density under typical initial reservoir pressure and temperature conditions: (i) runs involving bulk-phase (i.e., in the absence pore-walls) methane density measurements using a fixed number of methane molecules at fixed pressure temperature, and (ii) runs involving measurements of density of methane at the same temperature but confined to a pore with organic (graphite) walls. We will study deviations in the methane density of the second set of runs relative to the fixed density value of the bulk as an impact of the pore wall effects.

3.2. Molecular Dynamics Simulation of Methane Adsorption in Organic Slit-pores

For the molecular investigation, methane is considered at some supercritical condition under thermodynamic equilibrium in three-dimensional periodic orthorhombic pore geometry consisting of upper and lower pore-walls made of graphene (carbon) layers, see **Fig. 9**. For comparison, we take into account two slit-like pores with a pore width equal to H=3.6 nm (small pore) and H=1.95 nm (large pore) respectively. Pore width, H is an important length-scale of the study, which is defined as the distance between the centers-of-mass of the inner most graphene planes. The pores maintain fixed dimension in the y-coordinate: L_y=3.92nm; however, the dimension is changed in the x-coordinate such that both pores host the same number of methane molecules during the simulations. Hence, the dimensions in this direction are equal to L_x =4.26 nm and to L_x =7.67 nm for the large and small pores, respectively. A total of 400 methane molecules are typically used during the simulations.

A united-atom carbon-centered Lennard-Jones potential (based on the optimized potentials for liquid simulations, OPLS-UA force field), has been used as the model of a methane molecule, **Table 1** shows the energy and distance parameters used for fluid-fluid and solid-solid interactions.

The methane-solid and methane-methane interactions are of the Lennard-Jones type. Lorentz-Berthelot mixing rules: $\sigma_{ij}=(\sigma_{ii} + \sigma_{jj})/2$ and $\varepsilon_{ij}=(\varepsilon_{ii}\varepsilon_{jj})^{1/2}$ is set up in order to describe solid-fluid (i.e., pore-wall methane) interactions. Here, σ_{ij} and ε_{ij} are the Lennard-Jones parameters accounting for interactions between a molecular site of methane species and a carbon atom of the organic wall. Fluid-fluid interactions were cut off at 4σ=1.492 nm. Fluid-solid and fluid-fluid interactions were cut off at 5σ. The van der Waals interactions were cut off at 1.492 nm.

DL-POLY 2.20 was used to perform the molecular dynamics simulations. Methane bulk density computations are done considering isobaric and isothermic conditions (NPT) at three constant temperatures: T= [176, 212, 266] ºF, using Nosé-Hoover thermostat and barostat ensemble. The pressure was set up to a value corresponding to pore pressure at a particular run involving methane confined to pore. The relaxation time used in the ensembles was 35 picoseconds (ps) for the thermostat and 15 ps for the barostat.

In the case of simulations involving methane in carbon slit-pore, the initial the fluid system was equilibrated at a constant temperature, with an NVT ensemble using Berendsen thermostat algorithm. The equilibrium is assumed to be achieved if no drift in time was observed in the time-independent quantity, such as total energy of the system. After the equilibrium is reached, a new simulation is carried out in the canonical (NVT) ensemble using the Leapfrog algorithm (Frenkel and Smit, 2002; Allen and Tildesley, 2007) and Nosé-Hoover thermostat. Although Berendsen smoothly forces the fluid system to reach certain positions and velocity in which the temperature fluctuation is minimized, it is time-irreversible and the computations are not considered in canonical ensemble; the Nosé-Hoover algorithm needs to be used to control the system temperature while the real canonical ensemble computations are carried out for the density computations. The relaxation time used for the Nosé-Hoover thermostat is optimized to 25 ps. The values of the relaxation time needed to be optimized because values that are too small are known to cause high frequency temperature oscillations on the thermostat, whereas values that are too large lead to drift in temperature (Hünenberger, 2005). Typically, the total run time for a simulation was 1.5 nanoseconds and the time step used was 0.003 ps.

atom	σ(nm)	ε/k_B (K)
carbon	0.340	28.0
methane	0.373	147.9

Table 1. Lennard-Jones Potential Parameters for Methane and Carbon

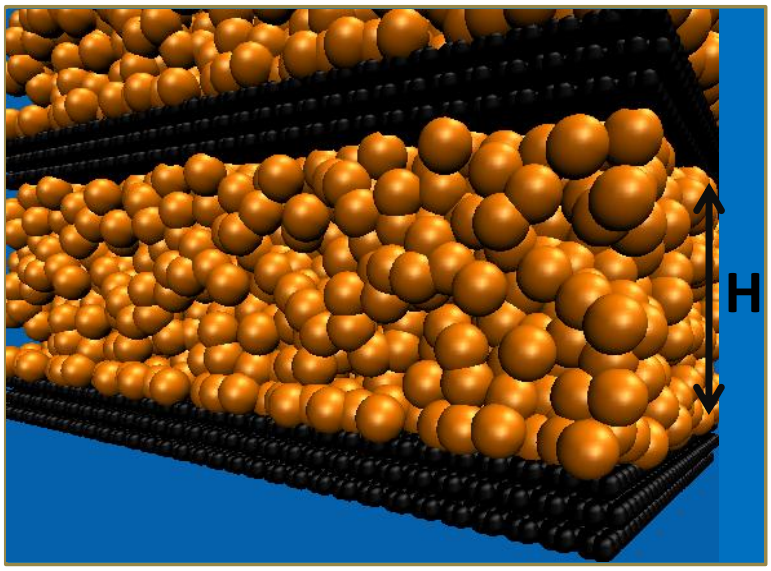

Fig. 9: Molecular simulation cell consisting of graphite walls and OPLS-UA methane

At the end of each simulation run, number density ρ_{Number} for methane across the pore space was computed at every 0.2 Å (for the continuous density profile) and at every 3.73 Å (for the discrete density profile) volume segment in the z-direction. The number density for each segment is estimated by counting the methane molecules across the volume $\Delta z L_x L_y$. Following, the number density is converted to the local mass density of methane using its molecular weight M_{CH4} and Avogadro's number as follows:

$$\rho_{CH_4} = \rho_{Number} M_{CH_4} / 6.02252 \times 10^{23}$$

As explained earlier, it is expected that the local mass density for methane across the pore will be different from its mean bulk density due to changing levels of interactions between the methane-methane and methane-carbon bodies. The purpose of our numerical investigation was to predict a precise density profile across the pore as an indication of the presence of these interactions and to determine an average adsorbed gas density value, a macroscopic quantity necessary for the gas in-place calculations using equation (13).

Fig. 10 shows two sets of mass density profiles for methane confined to pores with H=3.6 and 1.95 nm. It is clear that the predicted methane density is not uniform across the pores: it is significantly larger near the wall, where adsorption takes place, and decreases with damped oscillations as the distance from the pore wall is increased. The oscillations are due to presence of adsorption in the pores and involve structured distribution of molecules, i.e., molecular layers. The layers indicate existence of thermodynamic equilibrium in the pores. The number of molecules is largest in the first layer near the wall. The wall effect becomes significantly less in the second layer, indicating that desorption of some methane molecules is allowed due to equilibrium adsorption. The molecules in the second layer are still under the influence of pore walls although intermolecular interactions begin dominating, not allowing locally high methane densities. In this layer, the density of methane is slightly larger than the bulk gas density of methane under the same pressure and temperature, see **Table 2**.

3.2.1. Adsorption Layer Density. The molecular layer density of the first layer (one closest to the wall) is 0.48 and 0.57 g/cm^3 for the large and small pores, respectively. These values are above the range of densities corresponding to liquid methane. Note that the saturated orthobaric liquid methane density is within the range of 0.3-0.45 g/cm^3, whereas the experimentally measured adsorbed phase density values are also within the range of liquid density (Haydel and Kobayashi,

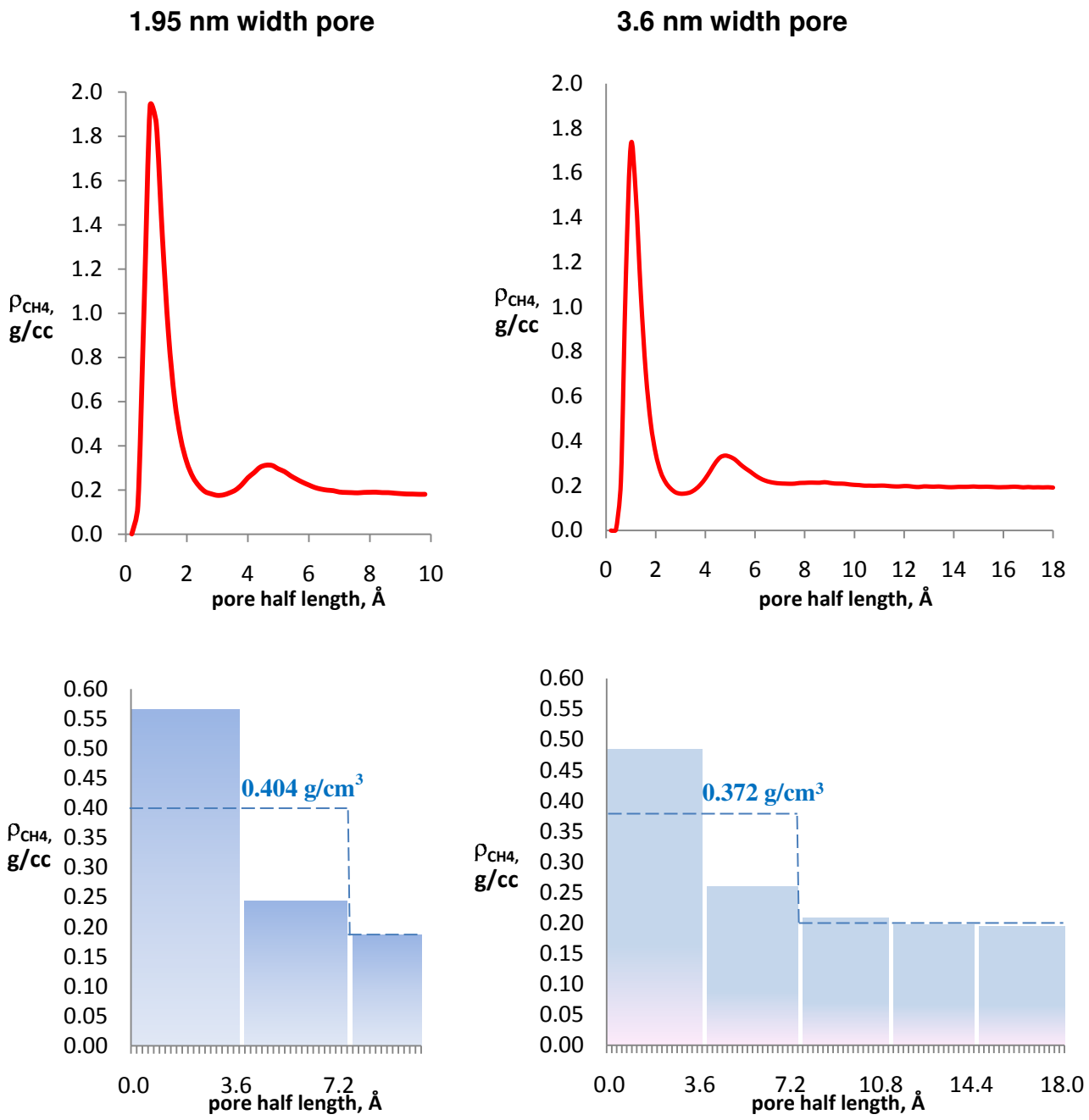

Fig. 10. Continuous (upper row) and discrete (lower row) density profiles for methane as a function of pore size at 176°F (80°C). Density values are estimated at 0.2 Å intervals for the continuous density profile. Discrete density corresponds to molecular layer density for methane across the pores. The dashed lines correspond to average values for the adsorbed phase density. The estimated pore pressure for the bulk phase measurements of methane with the pore width *H*=3.6nm is 4413 psi.

1967). The second molecular layer, on the other hand, represents a liquid/vapor transition in the pore with an average methane density 0.25 g/cm^3, which is lower (higher) than the saturated bulk liquid (gas) density. In this paper, being consistent with the Langmuir adsorption theory, we predicted the so-called "mono-layer" adsorbed phase density as the average of the first two layers by the wall. Hence, we averaged the molecular layer density values in between locations [0-7.46] Å in Fig. 10 (lower row) and determined an adsorbed-phase density equal 0.372 g/cm^3 for 3.6 nm pore and 0.404 g/cm for 1.95 nm pore. These are shown as step-wise dashed lines in the figure. Hence, an 8.6% increase is predicted in adsorption layer density due to 50% decrease in the pore size. These values show a moderate-level of dependence to the pore-size as well as a reasonably low range of values for the average macroscopic quantity in equation (13).

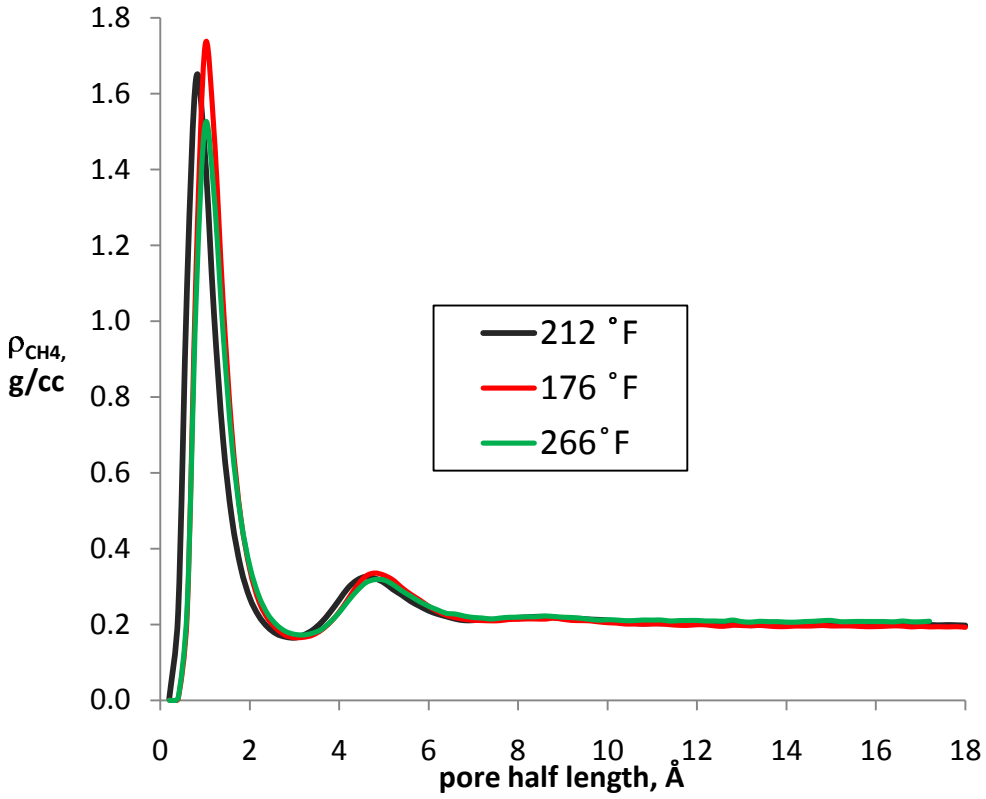

Fig. 11. Methane density profiles across half-length of a 3.6nm width slit-pore as a function of temperature.

Temperature: [˚F]	266	212	176
Ref. Density* : [g /cm^3]	0.19	0.17	0.16
MD Simulation: [g /cm^3]	0.20	0.18	0.165

Table 2. Estimated versus Reference values of bulk methane density
*** http://www.peacesoftware.de/einigewerte/methane.html**

3.2.2. Pore Size Effects on Methane Adsorption. In essence, supercritical methane in small organic pores is structured due to pore wall effects and shows layers of graded density across the pore. Depending on the pore size, a bulk fluid region may exist at the central portion of the pore, where the influence of molecular interactions with the pore walls is either very small or negligible. In pores with sizes up to 50 nm (Krishna, 2009) a combination of molecule-molecule and molecule-wall interactions dictates thermodynamic states of the gas and its mass transport in the pore. On the other hand, within a pore with a thickness less than 2 nm, methane molecules are always under the influence of the force field exerted by the walls; consequently, no bulk fluid region can be observed in the pore, therefore, behavior of the adsorbed molecules should be considered rather than the motion of free gas molecules.

3.2.1. Effect of Temperature on Methane Adsorption. The effect of temperature on methane density is shown in **Fig. 11**. The estimated average adsorbed methane density is 0.372 g/cm^3 at 176 ^{o}F, 0.368 g/cm^3 at 212 ^{o}F and 0.355 g/cm^3 at 266^{o}F. These values show variations within 5% due to changing levels of kinetic energy at the microscopic scale. These values are 1.86-2.0 times larger than methane bulk density at the center of the pore, which is a quantity not sensitive to pore temperature.

As a final remark of this section, we note that the estimated average adsorbed phase density values are in the same range with the experimental measurements of Haydel and Kobayashi, (1967).

4. Example

In order to quantify the pore-scale effects using the new methodology, we compare the results of the old method vs. the new method on two shales. The first shale has a low sorbed gas volume while the second has a relatively high sorbed gas volume. A value of 0.37 g/cm^3 is used for sorbed methane density based on the discussion in Section 3.2. The rest of the parameters for the two shales are as follows:

	Shale A: (low sorption capacity)	**Shale B: (high sorption capacity)**
ϕ	= 0.06	= 0.06
S_w	= 0.35	= 0.35
S_o	= 0.0	= 0.0
B_g	= 0.0046	= 0.0046
$\hat{M}$	= 20 lb/lb-mol	= 20 lb/lb-mol
G_{sL}	= 50 scf/ton	= 120 scf/ton
p	= 4000 psia	= 4000 psia
T	= 180 ^{o}F	= 180 ^{o}F
p_L	= 1150 psia	= 1800 psia
ρ_b	= 2.5 g/cm^3	= 2.5 g/cm^3
ρ_s	= 0.37 g/cm^3	= 0.37 g/cm^3

Using the old calculation method for gas-in-place the adsorbed, free, and total gas storage capacities for shale A are:

$$G_f = 32.0368\frac{\phi(1-S_w)}{\rho_b B_g} = 32.0368\frac{0.06(1-0.35)}{2.5\cdot 0.0046} = 108.6\ \text{scf/ton}$$

$$G_a = G_{sL}\frac{p}{p+p_L} = 50\frac{4000}{4000+1150} = 38.8\ \text{scf/ton}$$

$$G_{st} = G_f + G_a = 108.6\ \text{scf/ton} + 38.8\ \text{scf/ton} = 147.7\ \text{scf/ton}$$

Using the new calculation method for gas-in-place the free, sorbed, and total storage capacities for shale A are:

$$G_f = \frac{32.0368}{B_g}\left[\frac{\phi(1-S_w)}{\rho_b} - \frac{1.318\times 10^{-6}\hat{M}}{\rho_s}\left(G_{sL}\frac{p}{p+p_L}\right)\right]$$

$$= \frac{32.0368}{0.0046}\left[\frac{0.06(1-0.35)}{2.5} - \frac{1.318\times 10^{-6}\cdot 20}{0.37}\left(50\frac{4000}{4000+1150}\right)\right] = 89.4\ \text{scf/ton}$$

$$G_a = 50\frac{4000}{4000+1150} = 38.8\ \text{scf/ton}$$

$$G_{st} = 89.4\ \text{scf/ton} + 38.8\ \text{scf/ton} = 128.2\ \text{scf/ton}$$

This represents a decrease of 17.7% and 13.0 % of the free and total gas storage capacities respectively.

Using the old calculation method for gas-in-place the adsorbed, free, and total gas storage capacities for shale B are:

$$G_f = 32.0368\frac{\phi(1-S_w)}{\rho_b B_g} = 32.0368\frac{0.06(1-0.35)}{2.5\cdot 0.0046} = 108.6\ \text{scf/ton}$$

$$G_a = G_{sL}\frac{p}{p+p_L} = 120\frac{4000}{4000+1800} = 82.8\ \text{scf/ton}$$

$$G_{st} = G_f + G_a = 108.6\ \text{scf/ton} + 82.8\ \text{scf/ton} = 191.4\ \text{scf/ton}$$

Using the new calculation method for gas-in-place the free, sorbed, and total storage capacities for shale B are:

$$G_f = \frac{32.0368}{0.0046}\left[\frac{0.06(1-0.35)}{2.5} - \frac{1.318\times10^{-6}\cdot 20}{0.37}\left(120\frac{4000}{4000+1800}\right)\right] = 67.6\ \text{scf/ton}$$

$$G_a = 120\frac{4000}{4000+1800} = 82.8\ \text{scf/ton}$$

$$G_{st} = 67.6\ \text{scf/ton} + 82.8\ \text{scf/ton} = 150.4\text{scf/ton}$$

This represents a decrease of 37.8% and 21.4 % of the free and total gas storage capacities respectively.

5. Conclusion

In this paper we addressed the following issues in regards to the volume available for free gas in organic shales. The first question was what fraction of the pore volume of the organic material can be considered available for the free gas phase and what fraction is taken up by the adsorbed phase? This question was answered in that the current industry methodology is not taking into account the volume consumed by the sorbed phase. Additionally, it was shown that the sorbed phase follows Langmuir theory and that it takes up an approximately one-molecule thick portion of a pore, although there is a damped oscillation density profile. For a 100 nm pore, the volume is fairly insignificant; however, for pores on the order of a 10 nm, it is quite large.

The second question was, if a significant fraction of the organic pore volume is taken up by the adsorbed phase, how accurately is the shale gas storage capacity estimated using the conventional volumetric methods? We answered this question by showing that the current industry standard disregards the volume consumed by the sorbed phase, thus inadvertently overestimating the pore-volume available for free-gas storage. We showed that with equation (13) a more correct volume is calculated.

Finally we asked whether average densities exist for the free and the adsorbed phases and how large would a typical density contrast be in an organic pore for an accurate gas reserve calculation? Through MD simulation and Langmuir theory we showed that this density for methane typically equals 0.37g/cm^3. This value now corresponds to both experimental and numerical works and the value has little pressure or temperature dependence.

In conclusion, a robust method that matches the local physics is presented to determine an accurate estimate of the gas-in-place in organic-rich gas shale. Future work includes better estimation for the transport properties in the light of the new pore-scale findings.

Acknowledgements.

We recognize the work and contributions of Dr. Mark Curtis and Mr. Gary Stowe in collecting many of the images in this paper. We thank the staff at The University of Oklahoma's OSCER supercomputing center for the facilities to perform the MD simulations. We thank Devon Energy in particular Jerry Youngblood, Bret Jameson, Jeff Hall, Dr. Bill Coffey and Jan Glasgow for providing access to Barnett core and in support much of this work.

Nomenclature

B_g	gas formation volume factor, reservoir volume/surface volume
B_o	oil formation volume factor, reservoir volume/surface volume
B_w	water formation volume factor, reservoir volume/surface volume
G_a	adsorbed gas storage capacity, scf/ton
G'_a	Gibbs isotherm storage capacity, scf/ton
G_f	free gas storage capacity, scf/ton
G_{sL}	Langmuir storage capacity, scf/ton
G_{so}	dissolved gas-in-oil storage capacity, scf/ton
G_{sw}	dissolved gas-in-water storage capacity, scf/ton
H	pore size, Å
k_B	Boltzmann constant, 1.3806503×10^{-23} kJ/K^{-1}
L_x	length of computational cell in x-direction, Å
L_y	length of computational cell in y-direction, Å
$\hat{M}$	apparent natural gas molecular weight, lbm/lbmole
M_{CH4}	molecular weight of methane, g/mole
n	number of moles
p	pressure, psia

p_L	Langmuir pressure, psia
R_{so}	solution gas-oil ratio, scf/STB
R_{sw}	solution gas-water ratio, scf/STB
S_g	gas saturation, dimensionless
S_{ge}	effective gas saturation, dimensionless
S_o	oil saturation, dimensionless
S_w	water saturation, dimensionless
T	reservoir temperature, ^oF
V_b	bulk volume, ft^3
V_g	grain volume, ft^3
V_v	void volume, ft^3
V_{ve}	effective void volume, ft^3
V_{v0}	initial void volume, ft^3
V_{v1}	void volume step 1, ft^3
V_{v2}	void volume step 2, ft^3
Δz	interval across the pore space used for number density calculations, Å
ε	depth of the potential well, kJ
ϕ	total porosity fraction, dimenionless
ϕ_a	sorbed phase porosity fraction, dimenionless
ϕ_e	effective porosity fraction, dimensionless
ρ_b	bulk rock density, g/cm^3
ρ_{CH4}	mass density of methane in pore, g/cm^3
ρ_f	free gas phase density, g/cm^3
ρ_{Number}	number density of methane, number of molecules/ $Å^3$
ρ_s	sorbed phase density, g/cm^3
σ	distance at which the inter-molecular potential is zero, nm

References

1. Allen, M.P., and Tildesley, D.J. 2007. *Computer Simulation of Liquids*. Oxford University Press, London
2. Aukett, P.N.1992. Methane adsorption on Microporous Carbons – A Comparison of Experiment, Theory, and Simulation. *Carbon*, 30, 913-924.
3. Bustin R.M., Bustin A.M., Cui X., Ross D.J.K., Murthy Pathi V.S. 2008. Impact of Shale Properties on Pore Structure and Storage Characteristics. SPE-119892, paper presentation at the SPE Shale Gas Production Conference, Fort Worth, Texas, 16–18 November.
4. Cui, X., Bustin, A.M., and Bustin, R. 2009. Measurements of Gas Permeability and Diffusivity of Tight Reservoir Rocks: Different Approaches and Their applications. *Geofluids* 9, pp. 208-233.
5. Diaz-Campos, M., Akkutlu, I.Y., and Sigal, R.F. 2009. A Molecular Dynamics Study on Natural Gas Solubility Enhancement in Water Confined to Small Pores. SPE-124491, paper presented during the SPE Annual Technical Conference and Exhibition held in New Orleans, October 4-7.
6. Dubinin, MM. 1960. The Potential Theory of Adsorption of Gases and Vapors for Adsorbents with Enegetically Nonuniform Surfaces. *Chemical Review*, pp 235-241
7. Frenkel, D. and Smit B. 2002. *Understanding Molecular Simulation – From Algorithms to Applications*. Academic Press, Computational Science Series, San Diego
8. Ghoufi, A. 2009. Adsorption of CO_2, CH_4 and their Binary Mixture in Faujasite NaY: A Combination of Molecular Simulations with Gravimetry-manometry and Microcalorimetry Measurements. *Microporous and Mesoporous Materials*, 119, 117-128.
9. GRI (Gas Research Institute). *Coalbed Reservoir Gas in-place Analysis*, Gas Research Institute, Chicago. (1997)
10. Haydel, J., and Kobayashi, R. 1967. Adsorption Equilibria in the Methane-Propane-Silica Gel System at High Pressures. *Industrial and Engineering Chemistry Fundamentals*, Vol 6, pp. 564-554.
11. Harris J.G. 1995. Carbon Dioxide's Liquid-Vapor Coexistence Curve and Critical Properties as Predicted by a Simple Molecular Model. *J. Phys. Chem.,* 99, 12021-12024.
12. Hünenberger, P.H. 2005. Thermostat Algorithms for Molecular Dynamics Simulations. Adv. Polym. Sci., 173, 105-149.
13. Krishna R. 2009. Describing the Diffusion of Guest Molecules inside Porous Structures. *J. Phys. Chem. C,* 113, 19756-19781.
14. Loucks, R.G., Reed, R.M., Ruppel, S.C., and Jarvie, D.M. 2009. Morphology, Genesis, and Distribution of

Nanometer-Scale Pores in Siliceous Mudstones of the Mississippian Barnett Shale. *Journal of Sedimentary Research,* v. 79, pp. 848-861.
15. Luffel, D.L. and Guidry, F.K. 1992 New Core Analysis Methods for Measuring Rock Properties of Devonian Shale. *J. Petroleum Tech.* pp. 1184-1190.
16. Luffel, D.L., Hopkins, C.W., and Schettler, P.D. 1993. Matrix Permeability Measurement of Gas Productive Shales. SPE-26633, paper presented at the 68th Annual Tech. Conference & Exhibition, SPE, Houston, Texas, Oct. 3-6.
17. Mavor, M.J., Hartman, C., and Pratt, T.J. 2004. Uncertainty in Sorption Isotherm Measurements. Paper No 411, International Coalbed Methane Symposium, University of Alabama, Tuscaloosa.
18. Menon, P. G. 1968. Adsorption at High Pressures. *Chemical Reviews*, Vol 68, pp. 277-294.
19. Ming, L., Anzhong, G., Xuesheng, L., and Rongshun, W. 2003. Determination of the Adsorbate Density from Supercritical Gas Adsorption Equilibria Data. *Carbon* 41, pp. 585-588.
20. Ozawa, S., Kusumi, S., Ogino, Y. 1976. Physical Adsorption of Gases at High Pressure. *J. Colloid Interface Science,* 1976, pp 83-91.
21. de Pablo, J.J. and Escobedo, F.A. 2002. Molecular Simulations in Chemical Engineering: Present and future. *AICHEJ*, 48: 12 pp 2716-2721.
22. Sondergeld, C.H., Ambrose, R.J., Rai, C.S. and Moncrieff, J. 2009. Micro-Structural Studies of Gas Shales, SPE 131771-PP, SPE Unconventional Gas Conference, Pittsburg, PA 23-25 February 2010.
23. Tsai, M.C., Chen, W.N., Cen, P.L., Yang, R.T., Kornosky, R.M. 1985. Adsorption of Gas Mixture on Activated Carbon. *Carbon* 1985, Vol 23, pp 167-73.
24. Sweatman, M.B. and Quirke, N. 2001. Characterization of Porous Materials by Gas Adsorption: Comparison of nitrogen at 77 K and carbon dioxide at 298 K for activated carbon. Langmuir, 17:16 5011-5020.
25. Wang, F. P., Reed, R. M. 2009. Pore Networks and Fluid Flow in Gas Shales. SPE-124253, paper presented at the Annual Technical Conference and Exhibition, SPE, New Orleans, LA, October 4-7.
26. Yee, D., Seidle, J.P., and Hanson, W.B. 1993. Gas Sorption on Coal and Measurement of Gas Content. Law, B.E. and Rice D.D. (editors) *Hydrocarbons from Coal*, AAPG Studies in Geology #38, AAPG, Tulsa, OK (1993).

Appendix – Derivation of Equation (13)

Beginning with equation (5), the value G_a needs to be converted into a volume, a simple unit conversion can be performed. Typical unit of the equation below is scf/ton.

$$G_a = G_{sL}\frac{p}{p+p_L}$$

Given that it is in scf, we can convert scf into a mass with the ideal gas law at standard temperature and pressure:

$$V/n = RT/p$$

$$V/n = 10.7316\frac{\text{ft}^3\text{psi}}{^\circ\text{R lb - mol}}519.67^\circ\text{R}/14.696\text{ psia} = 379.48\frac{\text{ft}^3}{\text{lb - mol}}$$

With density in g/cm^3 and the desired units in scf/ton, we can use the above value to calculate a conversion constant.

$$\frac{1}{379.48\frac{\text{ft}^3}{\text{lb - mol}}}\cdot\frac{1\text{ ton}}{2000\text{ lb}} = 1.318\times10^{-6}\frac{\text{ton - mol}}{\text{ft}^3}$$

Using the conversion constant, the density of the adsorbed phase, the bulk density of the rock, and the molecular weight of the adsorbed phase we can calculate the fractional volume occupied by the sorbed phase.

$$\phi_a = 1.318\times10^{-6}\hat{M}\frac{\rho_b}{\rho_s}\left(G_{sL}\frac{p}{p+p_L}\right)$$

Assuming the oil saturation is negligible and taking the fractional sorbed-phase volume away from the free gas volume, equation (4) becomes:

$$G_f = 32.0368 \frac{\phi(1-S_w) - \phi_a}{\rho_b B_g}$$

Substituting the expression for ϕ_a into this equation and simplifying yields equation (13):

$$G_f = \frac{32.0368}{B_g}\left[\frac{\phi(1-S_w)}{\rho_b} - \frac{1.318\times10^{-6}\hat{M}}{\rho_s}\left(G_{sL}\frac{p}{p+p_L}\right)\right]$$